Rizk, Mohammad E.M.; Lehtonen, Matti; Baba, Yoshihiro; Abulanwar, Sayed

Performance of Large-Scale Grounding Systems in Thermal Power Plants Against Lightning Strikes to Nearby Transmission Towers

Published in:
IEEE Transactions on Electromagnetic Compatibility

DOI:
10.1109/TEMC.2018.2831700

Published: 01/04/2019

Document Version
Peer reviewed version

Please cite the original version:
Rizk, M. E. M., Lehtonen, M., Baba, Y., & Abulanwar, S. (2019). Performance of Large-Scale Grounding Systems in Thermal Power Plants Against Lightning Strikes to Nearby Transmission Towers. *IEEE Transactions on Electromagnetic Compatibility*, *61*(2), 400-408. [8365887]. https://doi.org/10.1109/TEMC.2018.2831700

Performance of Large-Scale Grounding Systems in Thermal Power Plants Against Lightning Strikes to Nearby Transmission Towers

Mohammad E. M. Rizk, Matti Lehtonen, *Member, IEEE*, Yoshihiro Baba, *Senior Member, IEEE*, and Sayed Abulanwar, *Member, IEEE*

***Abstract*—In spite of the contemporary interest in renewable power plants, thermal power plants are still inevitable. Various electric equipment and apparatus are grounded via a large-scale grounding system in thermal power plants. In this paper, the three-dimensional finite-difference time-domain method has been employed to study the performance of such a large-scale grounding system against a lightning strike to a nearby transmission tower. The study has emphasized how a nearby sea, which is utilized for cooling purposes in thermal power plants, influences the ground potential rise on the large-scale grounding system considering soil ionization. The results show that the distribution of the ground potential rise on the large-scale grounding system is quite dependent on the alignment of sea with the large-scale grounding system. In addition, the extent that soil ionization affects the ground potential rise is dependent on the distance between the struck tower and the large-scale grounding system.**

***Index Terms*—Electromagnetic fields, finite-difference time-domain (FDTD) method, grounding systems (GSs), lightning strikes.**

I. Introduction

THE GLOBAL interest in renewable energy is currently increasing due to environmental considerations. However, the majority of the contemporaneous electric energy consumed all over the world is actually produced from thermal power plants owing to the intermittent nature of renewable resources and their associated technical challenges [1]. Power system apparatus, equipment, and electric circuits inside a thermal power plant are grounded by a large-scale grounding system (LSGS) to protect them against power system electromagnetic transients such as lightning and switching surges. Therefore, a considerable research has been devoted to study grounding systems (GSs) [2], [3]. Effective design fundamentals of different GS configurations have been addressed [4], [5]. Moreover, the frequency dependence of soil parameters has been considered for the lightning response of grounding electrodes [6], [7]. Furthermore, the finite-difference time-domain (FDTD) method has been employed to study how the ground potential rise (GPR) spreads between two grounding electrodes in [8]. Recently, a design of a GS has been presented for substations considering inhomogeneous soil [9]. A measuring touch/step voltage technique is presented in [10] for GSs in substations. The high-frequency behavior of GSs has been considered to estimate the stress of the arresters [11].

The influence of soil inhomogeneity, in terms of both horizontal and vertical stratification of the ground, on lightning electromagnetic fields has been intensively investigated within the last few years, where the results exhibit such an influence to be quite significant [12]–[20]. In fact, not only soil inhomogeneity but also the phenomenon of soil ionization affects, in particular, the lightning response of GSs. Therefore, a considerable effort has been devoted to model this phenomenon and investigate its impact on the lightning response of GSs [21]–[24].

Due to the widespread of thermal power plants all over the world and since they are typically constructed close to a water body (e.g., sea or lake) for cooling purposes, we think that the lightning response of their LSGS still requires further investigation and analysis. Based on the above, important factors influence considerably the lightning response of those LSGS, such as the inhomogeneous resistivity because of the different media in ground and soil ionization associated with high electric fields around grounding electrodes. Furthermore, low-voltage control and communication circuits inside thermal power plants may be relatively long and, hence, grounded at different points of the LSGS. Accordingly, it is worth to analyze the performance of LSGSs against lightning strikes, as those circuits are quite vulnerable to lightning surges.

In this paper, transient electromagnetic fields are computed for the LSGS of a thermal power plant due to a lightning strike to a nearby grounded transmission tower, Twr, using the 3-D FDTD method. The nonlinearity and inhomogeneity of soil resistivity due to ionization and the different media composing the ground are considered. After introducing why such investigations are implemented in Section I, the adopted case studies

Manuscript received January 20, 2018; revised March 27, 2018; accepted April 7, 2018. *(Corresponding author: Mohammad E. M. Rizk.)*

M. E. M. Rizk and S. Abulanwar are with the Department of Electrical Engineering, Faculty of Engineering, Mansoura University, Mansoura 35516, Egypt (e-mail: eng_mohammad_2007@mans.edu.eg; abulanwar@mans.edu.eg).

M. Lehtonen is with the Department of Electrical Engineering and Automation, Aalto University, FI-00076 Espoo, Finland (e-mail: matti.lehtonen@aalto.fi).

Y. Baba is with the Department of Electrical Engineering, Doshisha University, Kyoto 610-0321, Japan (e-mail: ybaba@mail.doshisha.ac.jp).

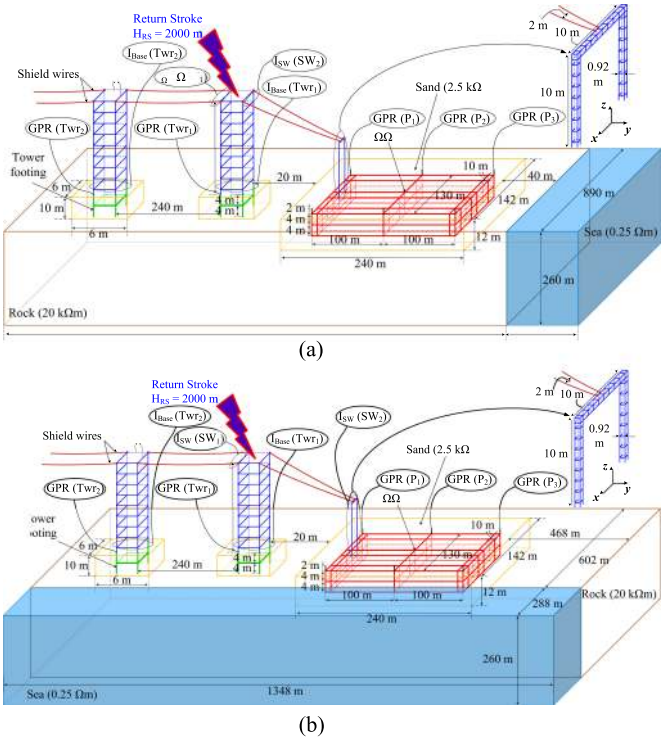

Fig. 1. Sea location for (a) CS_1 and (b) CS_2 configurations.

and the employed methodology to compute the electromagnetic transients are elaborated in Section II. Section III shows and analyzes the results of these computed electromagnetic transients, whereas their influence on relatively long circuits is discussed in Section IV. Finally, Section V explores the conclusions of this study. It is worth to mention that the back flashovers at the Twrs struck by lightning strikes are not considered, whereas this study emphasizes the computation of the GPR on the GSs of the Twrs and the LSGS.

II. Case Study and Methodology

An LSGS of a thermal power plant is considered with the closest two Twrs of the transmission system. The power plant is supposed to be on a rocky land so that the ground surface has been exploded and filled by a sand for the construction purposes. As aforementioned, the thermal power plant is constructed close to a sea for cooling. A return stroke is assumed to strike one of those Twrs that are connected together and to the gantry of the power plant via shielding wire, and the gantry is solidly connected to the LSGS.

A. Case Study

Two case studies, CS_1 and CS_2, are conceived regarding the position of the nearby sea, where it is located on the y^+ and x^+ sides of the LSGS for CS_1 and CS_2, respectively, as shown in Fig. 1. In addition, two striking scenarios, SC_1 and SC_2, are considered for each of CS_1 and CS_2, where the lightning strikes the first Twr, Twr_1, for the SC_1, as seen in Fig. 1, whereas the second Twr, Twr_2, is struck in SC_2. Fig. 1 shows that both

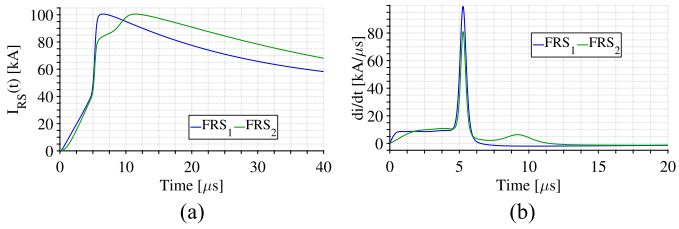

Fig. 2. (a) $I_{\mathrm{RS}}(t)$ and (b) di/dt of FRS_1 and FRS_2.

horizontal stratification and vertical stratification of the ground are included in this study owing to the existence of rock, sand, and sea, as illustrated before. The electrical properties for such different media are adopted as follows: the resistivity $\rho = 2500$, 20 000, and 0.25 Ω·m, whereas the relative permittivity $\epsilon_r = 10$, 4, and 40 for sand, rock, and sea, respectively. In fact, this work considers such values as the rocky ground has typically high ρ and low ϵ_r like the case in Nordic countries.

In Fig. 1, the radii of shield wires and grounding electrodes are, respectively, 0.004 and 0.01 m. The GS of each Twr has four vertical electrodes of 8 m in length and connected together under 4 m of the ground surface via horizontal electrodes. The LSGS consists of three layers of connected horizontal and vertical electrodes, where each electrode is separated by 10 m from the next parallel one. The LSGS dimensions are $130 \times 200 \times 8$ m^3 in the x-, y-, and z-axes, respectively, where the upper layer of the LSGS is at 2 m under the ground surface.

Two first stroke waveforms, FRS_1 and FRS_2, are adopted for the study, where FRS_1 has a single peak, while FRS_2 has a double peak. Both FRS_1 and FRS_2 have a velocity of 120 m/μs and rise to a peak I_P of 100 kA within a rise time $T_s = 6.5$ and 11.5 μs, respectively. Fig. 2 shows lightning current I_{RS} of both first stroke waveforms associated with their first time derivatives, di/dt. FRS_1 and FRS_2 have been conceived from the statistical observations of real lightning strokes to transmission towers shown in [25], where they are well compatible with cumulative probabilities of I_P, T_s, and di/dt.

Because of the high values of ρ adopted in this study, the ionization and deionization phenomena have been taken into account. Basically, when the electric fields produced around the grounding electrodes exceed a critical intensity, E_i, small air gaps between the soil particles around the electrodes start to ionize, and consequently, the equivalent ρ of the soil decreases. As long as the electric field intensity is higher than E_i, the ionization process continues and the equivalent ρ of the soil decreases more. On the other hand, such an ionization process stops when the electric field intensity becomes less than E_i, and subsequently, the equivalent ρ of the soil increases to restore its original value before the ionization, where such a case is known by the deionization process [21], [22].

B. Methodology

FRS_1 and FRS_2 have been modeled by the Heidler function (1) [26]. Heidler coefficients of both adopted current waveforms are obtained and given in Table I following the presented

TABLE I
HEIDLER'S COEFFICIENTS FOR FRS_1 AND FRS_2

k	FRS_1				FRS_2			
	I_{0k} (kA)	n_k	τ_{1k} (μs)	τ_{2k} (μs)	I_{0k} (kA)	n_k	τ_{1k} (μs)	τ_{2k} (μs)
1	8.96	2	0.96	80	7.7	2	2.4	60.8
2	15.36	3	2.4	80	11.55	3	2.8	20
3	9.28	5	3.84	20	7.7	5	4.16	16
4	13.12	7	4.8	48	9.76	7	4.8	48
5	53.44	36	5.28	35.2	34.92	44	5.28	48
6	35.2	2	80	480	28.24	2	8	480
7					14.63	15	9.36	38.8

approach in [27]. Furthermore, the stroke channel has been modeled using the transmission line model [28]

$$I_{RS}(t) = \sum_{k=1}^{K} \left(\frac{I_{0k}}{\eta_k} \cdot \exp\left(\frac{-t}{\tau_{2k}}\right) \cdot \left(\frac{t}{\tau_{1k}}\right)^{n_k} \div \left(1 + \left(\frac{t}{\tau_{1k}}\right)^{n_k}\right)\right) \tag{1a}$$

$$\eta_k = \exp\left(-\left(\tau_{1k}/\tau_{2k}\right) \cdot \left(n_k \cdot \tau_{2k}/\tau_{1k}\right)^{-n_k}\right). \tag{1b}$$

The 3-D FDTD method has been employed for this study to solve both Maxwell's curl equations, (2) and (3), numerically in the time domain. In fact, this method is quite advantageous in representing the inhomogeneous media of this study, as elaborated in Section II-A. Furthermore, the FDTD method tackles flexibly the ionization and deionization phenomena in the time domain without the need for predicting a specific volume of the ionized soil. Basically, the algorithm presented by Yee has been implemented to divide the solution space into orthogonal cells and position the electromagnetic fields within these cells along the Cartesian coordinates according to (2) and (3), whereas the electric and magnetic fields are alternatively updated following the Leapfrog approach [29]–[31]. Since the solution space, shown in Fig. 1, is relatively large, it has been nonuniformly divided, as elaborated in [30]. The electric fields located on the six boundary planes are differentially extrapolated using Liao second-order absorbing boundary conditions [32]. The shield wires and grounding electrodes are modeled using the thin-wire models illustrated in [33] and [34]. The shield wires are connected to the left absorbing boundary plane to avoid reflections [35]. Ultimately, the GPR and currents waveforms are, respectively, calculated by the line integral of the computed electric fields on the ground surface and using the Ampere law for the computed magnetic fields

$$\nabla \times \boldsymbol{E} = -\mu \cdot (\partial \boldsymbol{H}/\partial t) \tag{2}$$

$$\nabla \times \boldsymbol{H} = \sigma \cdot \boldsymbol{E} + \epsilon \cdot (\partial \boldsymbol{E}/\partial t) \tag{3}$$

where **E** and **H** are the electric field and magnetic field vectors; μ, σ, and ϵ are the permeability, conductivity, and permittivity of the medium, respectively; and $\partial/\partial t$ is the time-derivative operator.

In order to consider the ionization and deionization of soil in the 3-D FDTD method, ρ of each cell inside the soil has become a function of time depending on the resultant electric field $E = \sqrt{E_x^2 + E_y^2 + E_z^2}$ of the cell. The critical intensity of E to initiate ionization is taken as $E_i = 300$ kV/m. Thus, a cell inside soil ionizes, and its $\rho(t)$ decreases gradually as given by (4) for $E \geq E_i$ assuming ionization time constant, $\tau_i = 2\,\mu$s. The ionization process continues in such a cell as long as $E \geq E_i$ till its $\rho(t)$ reaches its minimal value ρ_i when $E = E_i$ at the end of the ionization. Afterwards, the deionization process begins as an ionized cell inside soil deionizes to restore its original value of $\rho(t)$, ρ_0, gradually as given by (5) for $E < E_i$ assuming deionization time constant, $\tau_d = 4.5\,\mu$s [21], [22]

$$\rho(t) = \rho_0 \cdot \exp\left(-t/\tau_i\right) \tag{4}$$

$$\rho(t) = \rho_i + (\rho_0 - \rho_i) \cdot (1 - \exp\left(-t/\tau_d\right)) \cdot (1 - E/E_i)^2. \tag{5}$$

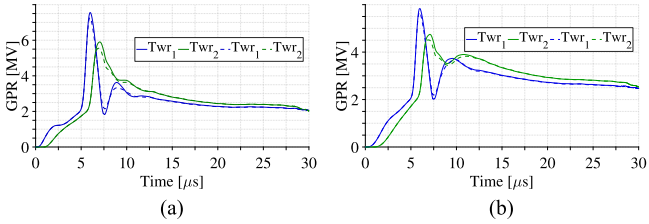

Fig. 3. GPR on Twr_1 and Twr_2 due to (a) FRS_1 and (b) FRS_2 for CS_1 and SC_1. (—— and - - - ⇒ without and with ionization.)

III. RESULTS AND ANALYSIS

The FDTD algorithm has been coded in the MATLAB platform, where the computer specifications are Intel Core i7-6700 with a 16-GB RAM. The computational time for a case including soil ionization is 5 h, and it becomes 2 h without ionization.

From the computed electric fields using the 3-D FDTD method, the GPR waveforms have been computed at points P_1, P_2, and P_3 of the LSGS as well as the two GSs of Twr_1 and Twr_2, as shown in Fig. 1. In addition, the current I_{Base} flowing through the bases of both Twr_1 and Twr_2 has been calculated from the computed magnetic fields in addition to the flowing current I_{SW} through the shield wires of the transmission system. As illustrated in Fig. 1, I_{SW} has been computed within the shield wires section from Twr_1 to Twr_2 and also the section from Twr_1 to the gantry.

Fig. 3 shows the calculated GPR waveforms for Twr_1 and Twr_2 due to FRS_1 and FRS_2 considering SC_1 and CS_1. It could be observed that FRS_1 having shorter T_s results in a higher GPR. Moreover, the soil ionization causes a decrease in the GPR due to the reduction in ρ of soil. For instance, the maximum values of the calculated GPR at Twr_1 and Twr_2 have, respectively, decreased by 3.8% and 6% due to soil ionization for FRS_1, and also by 2.7% and 5% for FRS_2. The GPR waveforms calculated at P_1, P_2, and P_3 due to FRS_1 and FRS_2 are presented in Fig. 4 considering SC_1 and CS_1. It is found that the influence of soil ionization on these GPR waveforms is quite slight. Moreover, the magnitudes of the GPR at P_1, P_2, and P_3 for FRS_1 are almost the same as their corresponding for FRS_2. Furthermore, the GPR distribution on P_1, P_2, and P_3 of the LSGS is nonuniform for either FRS_1 or FRS_2.

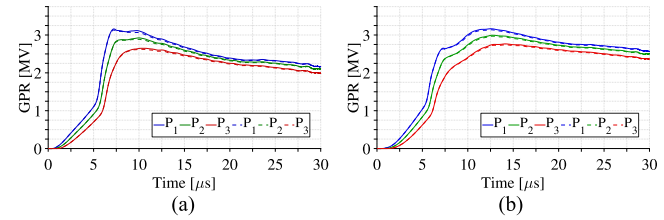

Fig. 4. GPR on P_1, P_2, and P_3 due to (a) FRS_1 and (b) FRS_2 for CS_1 and SC_1. (—— and - - - ⇒ without and with ionization.)

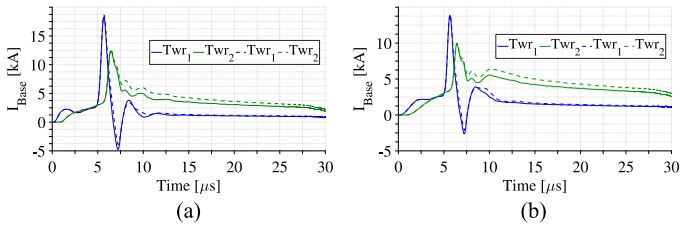

Fig. 5. I_{Base} due to (a) FRS_1 and (b) FRS_2 for CS_1 and SC_1. (—— and - - - ⇒ without and with ionization.)

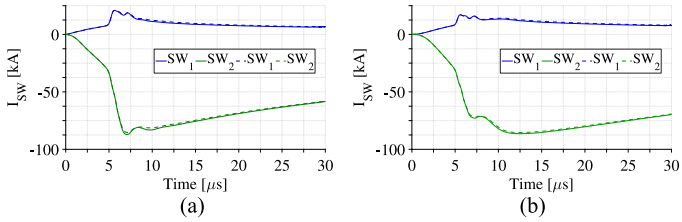

Fig. 6. I_{SW} due to (a) FRS_1 and (b) FRS_2 for CS_1 and SC_1. (—— and - - - ⇒ without and with ionization.)

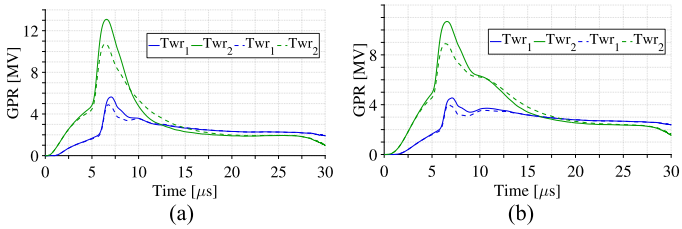

Fig. 7. GPR on Twr_1 and Twr_2 due to (a) FRS_1 and (b) FRS_2 for CS_1 and SC_2. (—— and - - - ⇒ without and with ionization.)

Fig. 5 shows the calculated I_{Base} for Twr_1 and Twr_2 due to both FRS_1 and FRS_2 considering the SC_1 and CS_1. In addition, Fig. 6 shows the calculated I_{SW} through the two portions, between Twr_1 and Twr_2 and between Twr_1 and the gantry, of the power plant. It could be observed from both Figs. 5 and 6 that the soil ionization causes an increase in I_{Base} and, consequently, a decrease in I_{SW} entering the gantry and, subsequently, the LSGS through the gantry. It is also deduced from these figures that most of I_{RS} flows through the shield wires portion between Twr_1 and the gantry due to the LSGS.

Figs. 7–10 are, respectively, the same as Figs. 3–6 but for SC_2. It is inferred from comparing Figs. 7–10 with Figs. 3–6 that the impact of soil ionization becomes more significant for SC_2 than SC_1. The maximum values of the computed GPR at Twr_1 and Twr_2 have, respectively, decreased by 18% and 13% due to soil ionization for FRS_1, and by 17% and 12% for FRS_2. This is because Twr_2 is farther located from the LSGS,

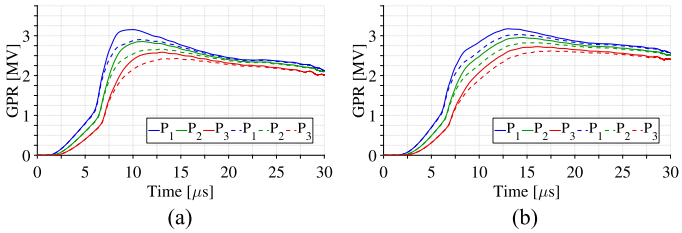

Fig. 8. GPR on P_1, P_2, and P_3 due to (a) FRS_1 and (b) FRS_2 for CS_1 and SC_2. (—— and - - - ⇒ without and with ionization.)

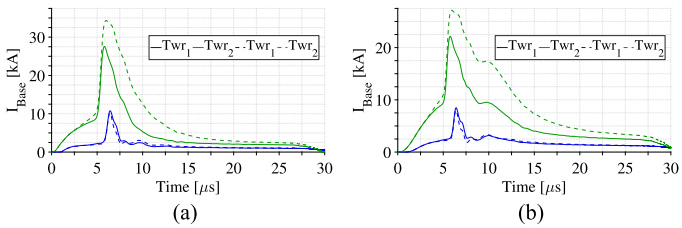

Fig. 9. I_{Base} due to (a) FRS_1 and (b) FRS_2 for CS_1 and SC_2. (—— and - - - ⇒ without and with ionization.)

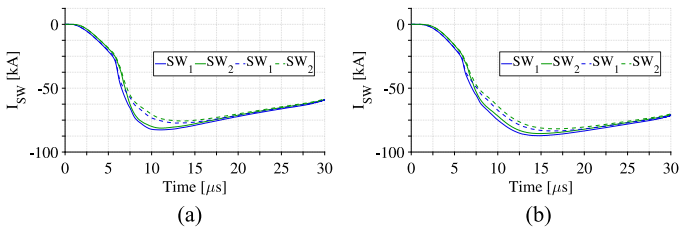

Fig. 10. I_{SW} due to (a) FRS_1 and (b) FRS_2 for CS_1 and SC_2. (—— and - - - ⇒ without and with ionization.)

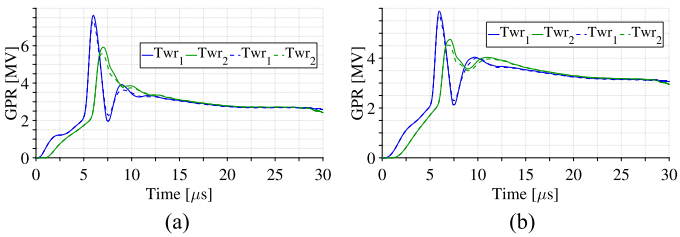

Fig. 11. GPR on Twr_1 and Twr_2 due to (a) FRS_1 and (b) FRS_2 for CS_2 and SC_1. (—— and - - - ⇒ without and with ionization.)

and subsequently, higher current flows through Twr_2, resulting in higher electric fields around its GS for SC_2. In addition, it is found that the computed I_{Base} for Twr_2 increases significantly due to such a considerable ionization of the soil around its GS for SC_2. Thereby, I_{SW} entering the LSGS through the gantry decreases considerably, thus resulting in lower magnitude of the GPR calculated at P_1, P_2, and P_3. Similar to SC_1, the magnitudes of the GPR waveforms at P_1, P_2, and P_3 are different for SC_2 with both FRS_1 and FRS_2. Ultimately, it is inferred that the GPR is nonuniform on the LSGS for CS_1 irrespective of the struck Twr, I_{RS}, and soil ionization.

Figs. 11–18 present the corresponding waveforms of those shown in Figs. 3–10, respectively, but for CS_2 depicted in Fig. 1(b). Considering SC_1, it is found from Fig. 11 that the maximum values of the computed GPR at Twr_1 and Twr_2 have, respectively, decreased due to soil ionization by 3.8% and

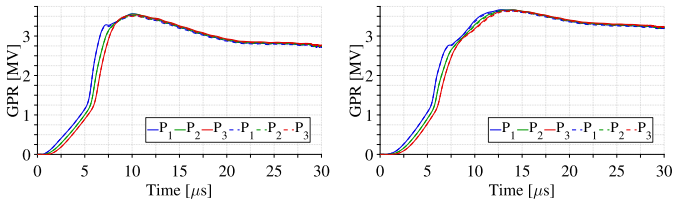

Fig. 12. GPR on P_1, P_2, and P_3 due to (a) FRS_1 and (b) FRS_2 for CS_2 and SC_1. (—— and - - - ⇒ without and with ionization.)

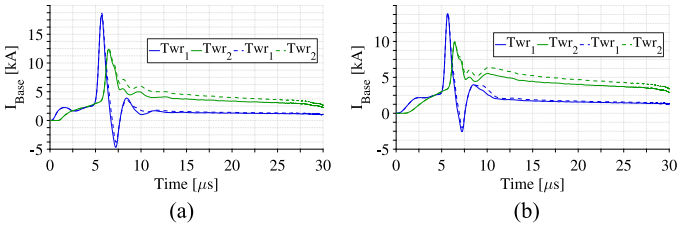

Fig. 13. I_{Base} due to (a) FRS_1 and (b) FRS_2 for CS_2 and SC_1. (—— and - - - ⇒ without and with ionization.)

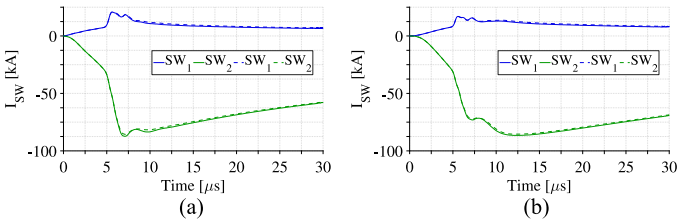

Fig. 14. I_{SW} due to (a) FRS_1 and (b) FRS_2 for CS_2 and SC_1. (—— and - - - ⇒ without and with ionization.)

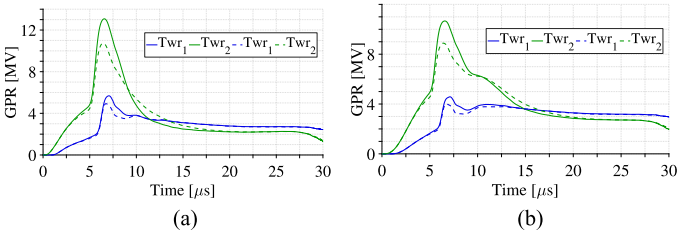

Fig. 15. GPR on Twr_1 and Twr_2 due to (a) FRS_1 and (b) FRS_2 for CS_2 and SC_2. (—— and - - - ⇒ without and with ionization.)

6% for FRS_1 and by 2.7% and 5% for FRS_2. Regarding SC_2, Fig. 15 exhibits that the maximum values of the computed GPR at Twr_1 and Twr_2 have, respectively, decreased due to soil ionization by 18% and 13% for FRS_1, and by 17% and 12% for FRS_2. Thereby, it is inferred that the reduction in the maximum values of the GPR calculated for both Twr_1 and Twr_2 owing to soil ionization is independent of the sea position, as the percentages of such a reduction for CS_1 are similar to their corresponding percentages for CS_2. It is found from Figs. 4, 8, 12, and 16 that the magnitudes of the GPR computed at P_1, P_2, and P_3 become almost equal for CS_2 in contrast to CS_1. This is attributed to that P_1, P_2, and P_3 are located on the same distance from the sea side (i.e., parallel to the sea side) so that the sea side, which represents a highly conductive surface, forces the GPR at those points to be the same. In this study, it is observed that the influence of soil ionization on GPR, I_{Base}, and I_{SW}

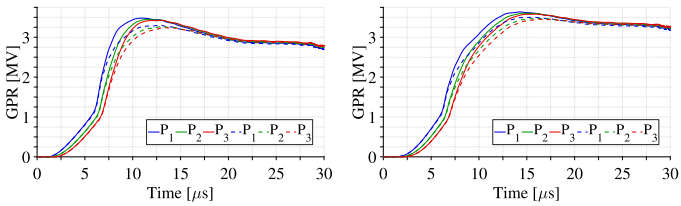

Fig. 16. GPR on P_1, P_2, and P_3 due to (a) FRS_1 and (b) FRS_2 for CS_2 and SC_2. (—— and - - - ⇒ without and with ionization.)

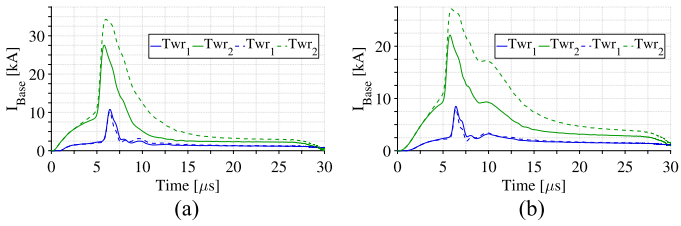

Fig. 17. I_{Base} due to (a) FRS_1 and (b) FRS_2 for CS_2 and SC_2. (—— and - - - ⇒ without and with ionization.)

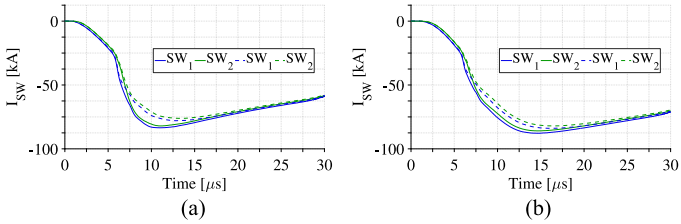

Fig. 18. I_{SW} due to (a) FRS_1 and (b) FRS_2 for CS_2 and SC_2. (—— and - - - ⇒ without and with ionization.)

waveforms is quite similar for both CS_1 and CS_2 depending on how far the struck Twr is from the LSGS as it becomes more significant for SC_2 as compared to SC_1.

It is worth to mention that the magnitudes of the GPR computed at P_1, P_2, and P_3 for CS_2 are higher than their corresponding magnitudes for CS_1 as noticed by comparing Figs. 12 and 16, respectively, with Figs. 4 and 8. Moreover, the differences between these GPR magnitudes for CS_2 and their corresponding magnitudes for CS_1 become greater and more significant with the closer points to the sea considering CS_1 (i.e., such differences are descendingly ordered from P_3, then P_2, and, finally, P_1). This observation is interpreted as follows: P_1, P_2, and P_3 are located along the y-axis so that their GPR waveforms are calculated by the line integral of the FDTD-computed perpendicular electric fields along the x-axis; since the sea is located on the y^+-direction of the LSGS for CS_1, then a considerable amount of the current flowing out of this GS tends to flow along the y-axis toward the sea side; such a behavior of the current flowing out of the LSGS results in lower electric fields along the x-axis, and consequently, the calculated GPR waveforms get lower. In fact, such an impact of the sea on the calculated GPR waveforms becomes surely more significant for the closer points to it so the GPR at P_3 is maximally influenced, then the GPR at P_2, and, finally, at P_1.

Fig. 19 shows the distribution of the horizontal electric field $E_r = \sqrt{E_x^2 + E_y^2}$ on the ground surface due to FRS_1 at 7 and

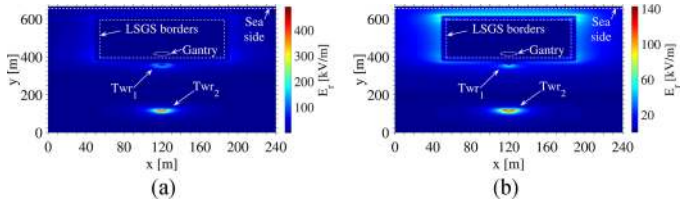

Fig. 19. Intensity of E_r on the ground surface due to FRS_1 at (a) 7 and (b) 21 μs for CS_1 and SC_1 considering soil ionization.

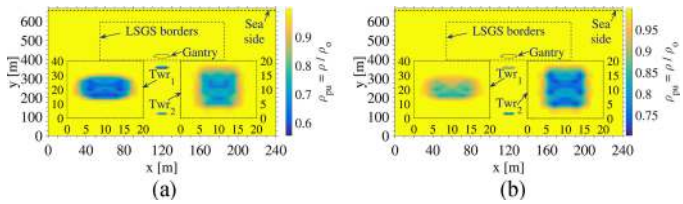

Fig. 20. Ionized area of soil on the ground surface due to FRS_1 at (a) 7 and (b) 21 μs for CS_1 and SC_1.

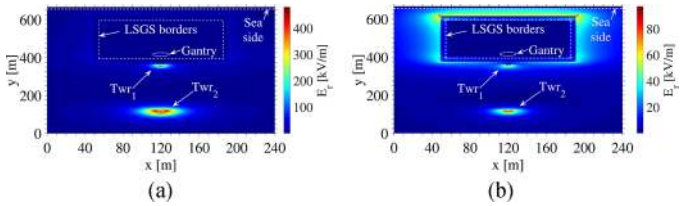

Fig. 21. Intensity of E_r on ground surface due to FRS_1 at (a) 7 and (b) 21 μs for CS_1 and SC_2 considering soil ionization.

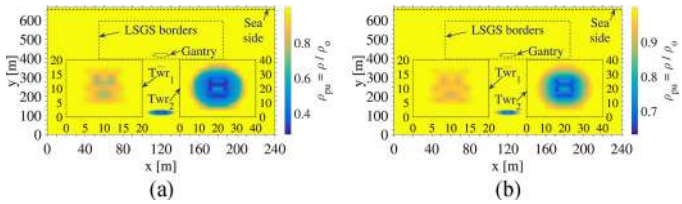

Fig. 22. Ionized area of soil on ground surface due to FRS_1 at (a) 7 and (b) 21 μs for CS_1 and SC_2.

21 μs for CS_1 and SC_1 considering soil ionization. It is shown from Fig. 19 that the distance between Twr_1 and Twr_2 is 240 m that conforms to Fig. 1. It is inferred from the figure that E_r on the ground surface inside the LSGS is zero because it is an equipotential surface. The maximal intensities of E_r are 490 and 140 kV/m at 7 and 21 μs, respectively. The intensity of E_r on the ground surface is descendingly graded from the LSGS and GSs of both Twrs to outside. The boundary conditions at the interfaces between different media, such as rock–sand and rock–sea, on the ground surface are verified. These boundary conditions are the continuity of the tangential electric field and perpendicular current density at the boundary. Since the sea is located on the y^+-direction of the LSGS for CS_1, the E_x components in the rock at the rock–sea boundary are forced to be zero owing to the continuity of the tangential electric field. On the other hand, the intensity of E_y components in the rock at the rock–sea boundary becomes considerably high owing to the continuity of the perpendicular current density as most of the current tends to flow toward the sea owing to its high σ. The boundary conditions are also verified at the rock–sand interface as shown around the LSGS in Fig. 19(b).

Fig. 20 shows the ionized area of soil on the ground surface due to FRS_1 at 7 and 21 μs considering CS_1 and SC_1. Owing to the different media on the ground surface (i.e., rock, sand, and sea), the ionized area is presented as a per-unit value of its original value before ionization, where $\rho_{pu} = \rho/\rho_0$. It could be observed from Fig. 20 that the soil has ionized around the GSs of both Twrs unlike the LSGS. This is attributed to that the current flows out of such an LSGS; it flows across a considerably large area, which results in low current density and, subsequently, low electric fields that are not sufficient and too low to cause soil ionization around the LSGS. The minimal values of ρ_{pu} on the ground surface are 0.56 and 0.7 at 7 and 21 μs, respectively. In Fig. 19, it could be deduced from the color bar that the electric field intensity on the ground surface at Twr_1 becomes lower than E_i so that the soil surrounding the GS of Twr_1 is deionizing at 7 μs and its ρ is increasing toward ρ_0. On the contrary, the electric field intensity on the ground surface at Twr_2 is higher than E_i so that the soil surrounding the GS of Twr_2 is ionizing at 7 μs and its ρ is decreasing. In addition, the electric field intensities on the ground surface at Twr_1 and Twr_2 are lower than E_i at 21 μs. Therefore, the minimal computed ρ_{pu} on the ground surface at 21 μs is greater than its corresponding one at 7 μs, as the soil is entirely deionizing at 21 μs. Ultimately, Figs. 19 and 20 exhibit conformance as both ionization and deionization processes are compatible with the electric field intensity. In order to further clarify the extension of the ionized area of soil on the ground surface, the ionized areas of soil around the GSs of Twr_1 and Twr_2 have been zoomed in the same figure, as shown in Fig. 20. It could also be noticed from Fig. 20 that the ionized area at Twr_1 shrinks with the passage of time as the soil is deionizing at 7 μs and beyond.

Figs. 21 and 22 are, respectively, the same as Figs. 19 and 20, but for SC_2. In Figs. 21 and 22, the maximal intensities of E_r are 480 and 97 kV/m, while the minimal ρ_{pu} are 0.28 and 0.63 at 7 and 21 μs, respectively. The comparison between Figs. 19 and 21 shows that the area of E_r exceeding E_i at the struck Twr is wider for SC_2 as compared to SC_1. This is because the current reaches the LSGS through the gantry for SC_1 much faster as compared to SC_2. Therefore, a greater amount of I_{RS} flows through the GS of Twr_2 in SC_2 as compared to that flows through the GS of Twr_1 in SC_1. In addition, it is particularly inferred from Fig. 21 that the boundary conditions at the rock–sand and rock–sea interfaces are verified. It is deduced from Figs. 20 and 22 that the ionized area of soil at the GS of the struck Twr is wider for SC_2 as compared to SC_1. In addition, the minimum value of ρ_{pu} for SC_2 is considerably lower than that for SC_1. In fact, the wider ionized area of soil and also the lower value of the minimum ρ_{pu} are attributed to the aforementioned greater amount of I_{RS} flowing through the GS of Twr_2 and the consequent higher electric fields for SC_2. Actually, such observations obtained from Figs. 20 and 22 reflect the greater influence of soil ionization on the computed GPR and current waveforms considering SC_2 as compared to SC_1, as presented

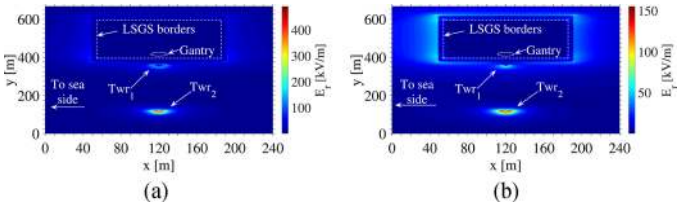

Fig. 23. Intensity of E_r on ground surface due to FRS_1 at (a) 7 and (b) 21 μs for CS_2 and SC_1 considering soil ionization.

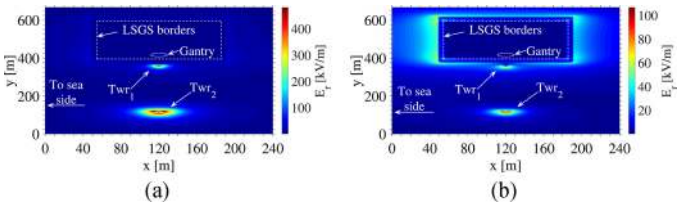

Fig. 24. Intensity of E_r on ground surface due to FRS_1 at (a) 7 and (b) 21 μs for CS_2 and SC_2 considering soil ionization.

before. It is also noticed from Fig. 22 that the ionized area of soil shrinks and ρ_{pu} increases with time passage due to the soil deionization.

Figs. 23 and 24 are, respectively, similar to Figs. 19 and 21, but for CS_2 rather than CS_1. In Fig. 23, the maximal intensities of E_r are, respectively, 490 and 160 kV/m at 7 and 21 μs, whereas their corresponding values are 480 and 105 kV/m in Fig. 24. Indeed, comparable observations are obtained from Figs. 19, 21, 23, and 24, while Figs. 23 and 24 differ from Figs. 19 and 21 regarding that E_r is no longer symmetrical with respect to mid-distance of the x-axis because the sea is located on the x^+ side of the LSGS. Accordingly, Figs. 23 and 24 show obviously that the intensity of E_r at the LSGS side facing the sea becomes greater as compared to the other side. This is justly due to that most of the current entering the LSGS tends to flow toward the sea because of its high σ.

The ionized area of soil on the ground surface for CS_2 has not been presented because it is identical to that for CS_1 shown in Figs. 20 and 22. This is due to that the GSs of Twr_1 and Twr_2, where the soil ionization happens, are sufficiently far from the sea side so that the electromagnetic fields in the vicinity of both GSs are not influenced by the reflections of the electromagnetic fields occurring at the sea–rock boundary.

IV. Discussion

This section discusses how different nonuniform and uniform GPR distributions on an LSGS affect the electrical stresses impinging a long low-voltage circuit having multigrounding points. As shown in Figs. 4, 8, 12, and 16, the GPR distribution is nonuniform for CS_1, while it is uniform for CS_2. Fig. 25 shows a long circuit of an aerial cable having l, r_1, r_2, r_3, $r_4 =$ 100, 0.0022, 0.004, 0.0044, 0.0048 m and $\epsilon_r = 4$ of the main insulator, $Ins._1$, whereas its ends are grounded to P_1 and P_2 of the LSGS. Such a circuit has been modeled deeming the frequency dependence for the cable parameters and its transformation matrix in an EMTP software. The GPR waveforms computed at P_1 and P_2 by the 3-D FDTD method considering soil ionization

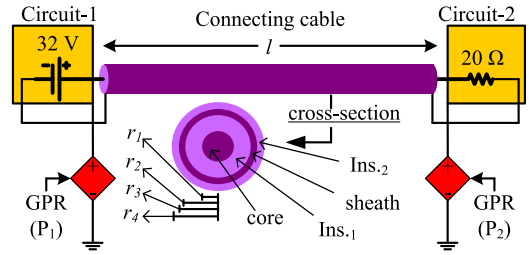

Fig. 25. Long circuit with multigrounding points on the LSGS.

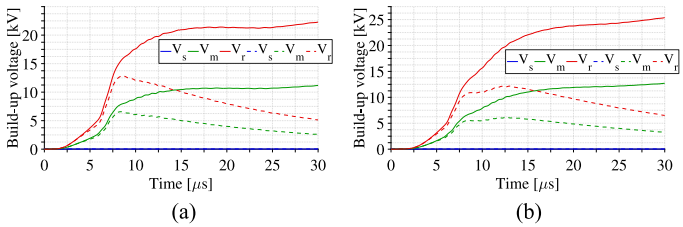

Fig. 26. Build-up voltage across $Ins._1$ due to (a) FRS_1 and (b) FRS_2 for SC_1 considering soil ionization. (—— and - - - ⇒ CS_1 and CS_2.)

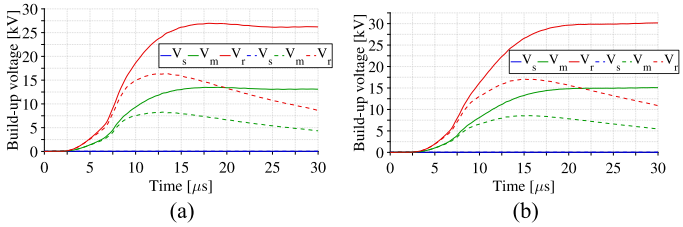

Fig. 27. Build-up voltage across $Ins._1$ due to (a) FRS_1 and (b) FRS_2 for SC_2 considering soil ionization. (—— and - - - ⇒ CS_1 and CS_2.)

have been exported to both controlled voltage sources of the circuit so that these sources exactly represent the GPRs at P_1 and P_2. A step voltage of 32 V is applied at the sending end of the cable, while the receiving end is matched by 20 Ω; such a configuration practically emulates a communication/control circuit between the protective devices or control center and the switchgear in power plants. Those electrical stresses are investigated in terms of the build-up voltages between the core and sheath (i.e., voltages across $Ins._1$) at both ends and the mid-point. Figs. 26 and 27 present the build-up voltages for SC_1 and SC_2, respectively, due to FRS_1 and FRS_2 at the sending end, V_s, mid-point, V_m, and the receiving end, V_r. These build-up voltages are shown in solid and dashed lines for CS_1 and CS_2, respectively. Figs. 26 and 27 show that $V_s = 32$ V for both CS_1 and CS_2. Moreover, it is obviously inferred that the nonuniform GPR distribution on the LSGS for CS_1 results in considerably higher V_m and V_r, as compared to the uniform GPR distribution for CS_2. It is also worth to mention that the nonuniform GPR distribution on the LSGS does not only cause high risk of failure for $Ins._1$, but also results in an increasing current through the cable sheath due to the potential difference between its two ends.

In [6], a dispersion of soil parameters has been reported, where σ increases and ϵ decreases with high-frequency components of the lightning current. Thereby, neglecting such frequency dependence of soil may overestimate the electric field at the ground level and, subsequently, indicate inaccurate

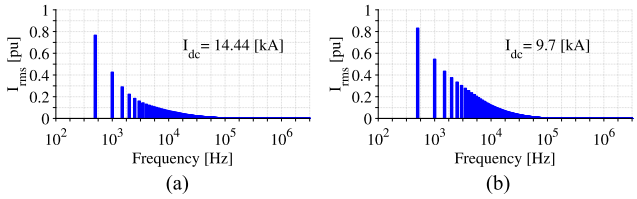

Fig. 28. Frequency spectrum in terms of $I_{\rm rms}/I_{\rm dc}$ for (a) FRS_1 and (b) FRS_2.

prediction of soil ionization, particularly for highly resistive soil [36]. Since the studied system includes quite high values of ρ, the frequency spectrum of FRS_1 and FRS_2 has been computed using the fast Fourier transform. The rms value of each frequency component, $I_{\rm rms}$, is presented as a ratio of the dc component, $I_{\rm dc}$, in Fig. 28. It is inferred that $I_{\rm rms}$ for frequency components $>10^4$ Hz is considerably low. Since σ varies slightly over a range up to around 10^4 Hz [6], we expect that such frequency dependence does not significantly affect the computation accuracy. Furthermore, the studied system is too complicated to include the frequency dependence of soil parameters due to the electromagnetic reflections between the Twr and its GS, the interactions between the GSs of the Twrs and the LSGS, and the nonlinearity and inhomogeneity of soil.

V. Conclusion

The response of an LSGS of a thermal power plant has been tackled for lighting strikes to nearby transmission towers, Twrs. The Twrs are connected to the LSGS via shield wires and the plant gantry. The impacts of nearby sea, distance between the struck Twr and the LSGS, and soil ionization on such a lightning response have been considered. The results reveal a remarkable impact of sea on the propagation of electromagnetic fields through the LSGS and, subsequently, the distribution of the GPR on the LSGS owing to its high conductivity. It is also inferred that low-voltage control and communication circuits, having multigrounding points of the LSGS, are liable to nonuniform GPR distribution that causes destructive effects. Accordingly, it is recommended for the grounding points of such circuits to be parallel to the sea side for uniform GPR distribution at those points so as to avoid severe electrical stresses. The results show that the soil around the GSs of Twrs is potentially exposed to ionization unlike that in the LSGS vicinity. Soil ionization causes a decrease in the soil resistivity and, subsequently, the computed GPR. The farther the struck Twr is from LSGS, the ionization impact on the GPR and currents waveforms becomes more significant.

References

[1] A. Clerici, "World energy resources," World Energy Council, London, U.K., Tech. Rep., 2016. [online]. Available: https://www.worldenergy.org/publications/2016/world-energy-resources-2016/

[2] G. Ala and M. L. Di Silvestre, "A simulation model for electromagnetic transients in lightning protection systems," *IEEE Trans. Electromagn. Compat.*, vol. 44, no. 4, pp. 539–554, Nov. 2002.

[3] R. G. Olsen and L. Grcev, "Analysis of high-frequency grounds: Comparison of theory and experiment," *IEEE Trans. Ind. Appl.*, vol. 51, no. 6, pp. 4889–4899, Nov./Dec. 2015.

[4] R. H. Kaufmann, "Some fundamentals of equipment-grounding circuit design," *AIEE Trans.*, vol. 73, pp. 267–270, 1954.

[5] M. O. Durham, "Grounding system design for isolated locations and plant systems," *IEEE Trans. Ind. Appl.*, vol. 33, no. 2, pp. 374–382, Mar./Apr. 1997.

[6] R. Alipio and S. Visacro, "Modeling the frequency dependence of electrical parameters of soil," *IEEE Trans. Electromagn. Compat.*, vol. 56, no. 5, pp. 1163–1171, Oct. 2014.

[7] R. Alipio and S. Visacro, "Time-domain analysis of frequency-dependent electrical parameters of soil," *IEEE Trans. Electromagn. Compat.*, vol. 59, no. 3, pp. 873–878, Jun. 2017.

[8] K. Yamamoto, T. Ookawa, and S. Sumi, "Study of the spread of potential rise between two grounding electrodes," *IEEE Trans. Ind. Appl.*, vol. 51, no. 6, pp. 5247–5253, Nov./Dec. 2015.

[9] P. Kapijan, S. Potivejkul, and P. Yutthagowith, "Grounding system design of substation using Matlab program," in *Proc. Int. Elect. Eng. Congr.*, 2017, pp. 1–4.

[10] G. Parise, L. Parise, L. Martirano, F. Tummolillo, G. Vagnati, and A. Barresi, "Tests and monitoring of grounding systems in HV/MV substations," *IEEE Trans. Ind. Appl.*, vol. 53, no. 2, pp. 929–935, Mar./Apr. 2017.

[11] R. Shariatinasab, J. Gholinezhad, and K. Sheshyekani, "Estimation of energy stress of surge arresters considering the high-frequency behavior of grounding systems," *IEEE Trans. Electromagn. Compat.*, vol. 60, no. 4, pp. 917–925, Aug. 2018.

[12] J. Paknahad, K. Sheshyekani, and F. Rachidi, "Lightning electromagnetic fields and their induced currents on buried cables. Part I: The effect of an ocean–land mixed propagation path," *IEEE Trans. Electromagn. Compat.*, vol. 56, no. 5, pp. 1137–1145, Oct. 2014.

[13] J. Paknahad, K. Sheshyekani, F. Rachidi, and M. Paolone, "Lightning electromagnetic fields and their induced currents on buried cables. Part II: The effect of a horizontally stratified ground," *IEEE Trans. Electromagn. Compat.*, vol. 56, no. 5, pp. 1146–1154, Oct. 2014.

[14] J. O. S. Paulino, C. F. Barbosa, and W. do Couto Boaventura, "Lightning-induced current in a cable buried in the first layer of a two-layer ground," *IEEE Trans. Electromagn. Compat.*, vol. 56, no. 4, pp. 956–963, Aug. 2014.

[15] C. F. Barbosa, J. O. S. Paulino, and W. do Couto Boaventura, "A time-domain method for the horizontal electric field calculation at the surface of two-layer earth due to lightning," *IEEE Trans. Electromagn. Compat.*, vol. 55, no. 2, pp. 371–377, Apr. 2013.

[16] Q. Zhang, X. Tang, J. Gao, L. Zhang, and D. Li, "The influence of the horizontally stratified conducting ground on the lightning-induced voltages," *IEEE Trans. Electromagn. Compat.*, vol. 56, no. 2, pp. 435–443, Apr. 2014.

[17] Q. Zhang, X. Tang, W. Hou, and L. Zhang, "3-D FDTD simulation of the lightning-induced waves on overhead lines considering the vertically stratified ground," *IEEE Trans. Electromagn. Compat.*, vol. 57, no. 5, pp. 1112–1122, Oct. 2015.

[18] A. Mimouni, F. Rachidi, and M. Rubinstein, "Electromagnetic fields of a lightning return stroke in presence of a stratified ground," *IEEE Trans. Electromagn. Compat.*, vol. 56, no. 2, pp. 413–418, Apr. 2014.

[19] S. Fortin, N. Mitskevitch, and F. P. Dawalibi, "Analysis of grounding systems in horizontal multilayer soils containing finite heterogeneities," *IEEE Trans. Ind. Appl.*, vol. 51, no. 6, pp. 5095–5100, Nov./Dec. 2015.

[20] M. E. Rizk, F. Mahmood, M. Lehtonen, E. A. Badran, and M. H. Abdel-Rahman, "Induced voltages on overhead line by return strokes to grounded wind tower considering horizontally stratified ground," *IEEE Trans. Electromagn. Compat.*, vol. 58, no. 6, pp. 1728–1738, Dec. 2016.

[21] A. Liew and M. Darveniza, "Dynamic model of impulse characteristics of concentrated earths," *Proc. Inst. Elect. Eng.*, vol. 121, no. 2, pp. 123–135, 1974.

[22] G. Ala, P. Buccheri, P. Romano, and F. Viola, "Finite difference time domain simulation of earth electrodes soil ionisation under lightning surge condition," *IET Sci., Meas. Technol.*, vol. 2, no. 3, pp. 134–145, 2008.

[23] G. Ala, M. L. Di Silvestre, F. Viola, and E. Francomano, "Soil ionization due to high pulse transient currents leaked by earth electrodes," *Prog. Electromagn. Res. B*, vol. 14, pp. 1–21, 2009.

[24] K. Otani, Y. Baba, N. Nagaoka, A. Ametani, and N. Itamoto, "FDTD surge analysis of grounding electrodes considering soil ionization," *Elect. Power Syst. Res.*, vol. 113, pp. 171–179, 2014.

[25] J. Takami and S. Okabe, "Observational results of lightning current on transmission towers," *IEEE Trans. Power Del.*, vol. 22, no. 1, pp. 547–556, Jan. 2007.

[26] F. Heidler and J. Cvetić, "A class of analytical functions to study the lightning effects associated with the current front," *Eur. Trans. Electr. Power*, vol. 12, no. 2, pp. 141–150, 2002.

[27] A. De Conti and S. Visacro, "Analytical representation of single-and double-peaked lightning current waveforms," *IEEE Trans. Electromagn. Compat.*, vol. 49, no. 2, pp. 448–451, May 2007.
[28] Y. Baba and V. Rakov, "On the transmission line model for lightning return stroke representation," *Geophys. Res. Lett.*, vol. 30, no. 24, 2003.
[29] K. Yee, "Numerical solution of initial boundary value problems involving maxwell's equations in isotropic media," *IEEE Trans. Antennas Propag.*, vol. 14, no. 3, pp. 302–307, May 1966.
[30] A. Taflove and S. C. Hagness, *Computational Electrodynamics: The Finite-Difference Time-Domain Method*. Norwood, MA, USA: Artech House, 2005.
[31] Y. Baba and V. A. Rakov, *Electromagnetic Computation Methods for Lightning Surge Protection Studies*. Hoboken, NJ, USA: Wiley–IEEE Press, 2016, p. 309.
[32] Z.-F. Liao, K.-L. Huang, B.-P. Yang, and Y.-F. Yuan, "A transmitting boundary for transient wave analyses," *Sci. China Ser. A, Math., Phys., Astronomy Technol. Sci.*, vol. 27, no. 10, pp. 1063–1076, 1984.
[33] T. Noda and S. Yokoyama, "Thin wire representation in finite difference time domain surge simulation," *IEEE Trans. Power Del.*, vol. 17, no. 3, pp. 840–847, Jul. 2002.
[34] Y. Baba, N. Nagaoka, and A. Ametani, "Modeling of thin wires in a lossy medium for FDTD simulations," *IEEE Trans. Electromagn. Compat.*, vol. 47, no. 1, pp. 54–60, Feb. 2005.
[35] A. Tatematsu and T. Noda, "Three-dimensional FDTD calculation of lightning-induced voltages on a multiphase distribution line with the lightning arresters and an overhead shielding wire," *IEEE Trans. Electromagn. Compat.*, vol. 56, no. 1, pp. 159–167, Feb. 2014.
[36] R. Alipio, M. Schroeder, M. Afonso, T. Oliveira, and S. Assis, "Electric fields of grounding electrodes with frequency dependent soil parameters," *Electr. Power Syst. Res.*, vol. 83, no. 1, pp. 220–226, 2012.

Mohammad E. M. Rizk received the B.Sc. and M.Sc. degrees in electrical engineering from Mansoura University, Mansoura, Egypt, in 2007 and 2011, respectively, and the D.Sc. degree from Aalto University, Espoo, Finland, in 2016.

He joined the Department of Electrical Engineering and Automation, Aalto University, as a Postdoctoral Researcher in 2017. He is currently an Assistant Professor of electrical engineering with Mansoura University. His research interests include power system transients, lightning overvoltages in power systems, and transient electromagnetic fields.

Matti Lehtonen (M'11) received the Master's and Licentiate degrees in electrical engineering from the Helsinki University of Technology, Espoo, Finland, in 1984 and 1989, respectively, and the Doctor of Technology degree from the Tampere University of Technology, Tampere, Finland, in 1992.

He was with VTT Energy, Espoo, Finland, from 1987 to 2003. Since 1999, he has been a Professor of power systems and high-voltage engineering with Aalto University, Espoo. His main research interests include power system planning and asset management, power system protection including earth fault problems, and harmonic-related issues.

Yoshihiro Baba (S'95–M'99–SM'13) received the B.Sc., M.Sc., and Ph.D. degrees from the University of Tokyo, Tokyo, Japan, in 1994, 1996, and 1999, respectively.

In 1999, he joined Doshisha University, Kyoto, Japan, where he has been a Professor since 2012. From April 2003 to August 2004, he was a Visiting Scholar with the University of Florida, Gainesville, FL, USA, on sabbatical leave from Doshisha University. He has authored or coauthored more than 70 papers published in reviewed journals.

Dr. Baba was a Distinguished Reviewer of the IEEE TRANSACTIONS ON ELECTROMAGNETIC COMPATIBILITY in 2013, 2014, and 2015. He was a recipient of the Technical Achievement Award from the IEEE Electromagnetic Compatibility Society in 2014. He is the Chairperson of Technical Program Committee of the 2015 Asia-Pacific International Conference on Lightning (APL), Nagoya, Japan. He has been the Vice Chairperson of the APL Steering Committee since 2017. He is the Convener of C4.37 Working Group of the International Council on Large Electric Systems. He has been an Editor for the IEEE TRANSACTIONS ON POWER DELIVERY since 2009. He is a Fellow of the Institution of Engineering and Technology.

Sayed Abulanwar (S'12–M'16) received the B.Sc. and M.Sc. degrees in electrical engineering from Mansoura University, Mansoura, Egypt, in 2005 and 2010, respectively, and the Ph.D. degree from Aalborg University, Aalborg, Denmark, in 2016.

He is currently an Assistant Professor of electrical engineering with Mansoura University. His research interests include wind turbine control, high-voltage direct-current systems, and transients in power systems.